Disturbance Observer and Nonlinear Damping Control for Fast Tracking Quadrotor Vehicles

Aurlio T. Salton[1], Diego Eckhard[2], Jeferson V. Flores[3], Guilherme Fernandes[1] and Guilherme Azevedo[1]

***Abstract*— This paper considers the design and implementation of a discrete-time fast tracking controller for quadrotor vehicles subject to perturbations. The proposed controller consists of a model-based disturbance observer and a Composite Nonlinear Feedback (CNF) controller. The CNF control law introduces nonlinear damping to the system so that it possesses a fast rise time without overshoot. The least square identification method is applied to develop a model based disturbance observer, thus decoupling the problems of track following and disturbance rejection. Experimental results are provided in order to validate the proposed approach.**

I. INTRODUCTION

From environmental surveys [1], [2] and pollution monitoring [3], to agriculture and meteorological data acquisition [4], [5], Unmanned Aerial Vehicles (UAVs) have presented themselves as a promising technology with the potential to significantly contribute to several interdisciplinary applications. Naturally, there are many other applications that may benefit from UAVs, among which the monitoring of power lines [6], wireless network integration [7], tridimensional real time mapping [8] and surveillance systems [9] are already being explored. While the number of potential applications to UAVs is already significant, it is certainly growing by the day.

Among the commonly employed UAVs, the so-called quadrotor has gained particularly attention due to its versatility and simple construction. This vehicle comprises four independent rotating blades that allow the system to take off and land vertically, which makes it more attractive than fixed wing UAVs for a number of different applications [10]. These and many other benefits inherent to quadrotors gave rise to several of the so called flying arenas, such as the ones at Stanford [11], MIT [12] and the Institute of Dynamic Systems & Control (IDSC), at Zurique [13].

While numerical advanced methods for the control of these vehicles are being implemented – such as Nonlinear Model Predictive Control (NMPC) [14] – computationally efficient solutions encompassing advanced controllers are still rare in the literature. This is no surprise given the difficulty of controlling these systems, since they are nonlinear, multivariable and underactuated. However, the quadrotor control problem may be significantly simplified when hierarchically divided. Normally, the tasks of altitude and angular position are considered in separate and individually controlled by independent PID controllers [10]. Needless to say, the PID strategy is a logical first choice for the control of these vehicles due to the simplicity and satisfactory performance it achieves. However, there are many advanced nonlinear techniques that could replace the classic PID controller and provide a significant better performance to the UAV control.

The main objective of this paper is the design and implementation of a computationally efficient high performance controller for fast tracking quadrotor vehicles. Given this scenario, the Composite Nonlinear Feedback (CNF) [15] controller, also known as dynamic damping control [16], will be adapted from its original form [17] and implemented to the system at hand. As shown in [15] this technique is able to achieve a performance similar to that given by time-optimal controllers, without suffering from the effects of chattering.

This paper is organized in the following manner: Section II presents the problem definition and the system identification; a disturbance rejection strategy is presented in section Section III followed by the proposed nonlienar control described in Section IV; experimental results are shown in Section V and concluding remarks are given in Section VI.

II. PRELIMINARIES

A. Problem Definition

The quadrotor vehicle considered in this paper is modeled by four dynamic equations given by,

$$\begin{array}{rcl} \ddot{\theta} & = & I_\theta(v_1 - v_3) - b_\theta\dot{\theta} + f_\theta, \\ \ddot{\phi} & = & I_\phi(v_4 - v_2) - b_\phi\dot{\phi} + f_\phi, \\ \ddot{\psi} & = & I_\psi(v_1 + v_3 - v_2 - v_4) - b_\psi\dot{\psi} + f_\psi, \\ \ddot{z} & = & \frac{1}{M}(v_1 + v_2 + v_3 + v_4) - b_z\dot{z} + f_z, \end{array} \quad (1)$$

where, θ and ϕ describe the roll and pitch angles, and ψ and z represent yaw and height, respectively. Variables $v_i,\ i = 1...4$ are the upward facing forces generated by each motor-blade pair and $I_{\theta,\phi,\psi,z}$ are constructive constants. Furthermore, $b_{\theta,\phi,\psi,z}$ are the kinetic friction constants, M is the mass of the vehicle and $f_{\theta,\phi,\psi,z}$ represent external disturbance forces along with unmodeled coupling dynamics. These equations allow the separation of the different control tasks such that each motor control law is given as follows:

$$\begin{array}{rcl} v_1(t) & = & v_z(t) + v_\theta(t) + v_\psi(t), \\ v_2(t) & = & v_z(t) - v_\phi(t) - v_\psi(t), \\ v_3(t) & = & v_z(t) - v_\theta(t) + v_\psi(t), \\ v_4(t) & = & v_z(t) + v_\phi(t) - v_\psi(t), \end{array} \quad (2)$$

[1]PUCRS - Faculdade de Engenharia Av. Ipiranga, 6681, 90619-900, Porto Alegre, RS, Brasil aurelio.salton@pucrs.br

[2]UFRGS - Departamento de Matemática Pura e Aplicada Av. Bento Gonalves 9500, 91509-900, Porto Alegre, RS, Brasil diegoeck@ufrgs.br

[3]UFRGS - Departamento de Engenharia Elétrica Av. Osvaldo Aranha 103, 90035-190, Porto Alegre, RS, Brasil jeferson.flores@ufrgs.br

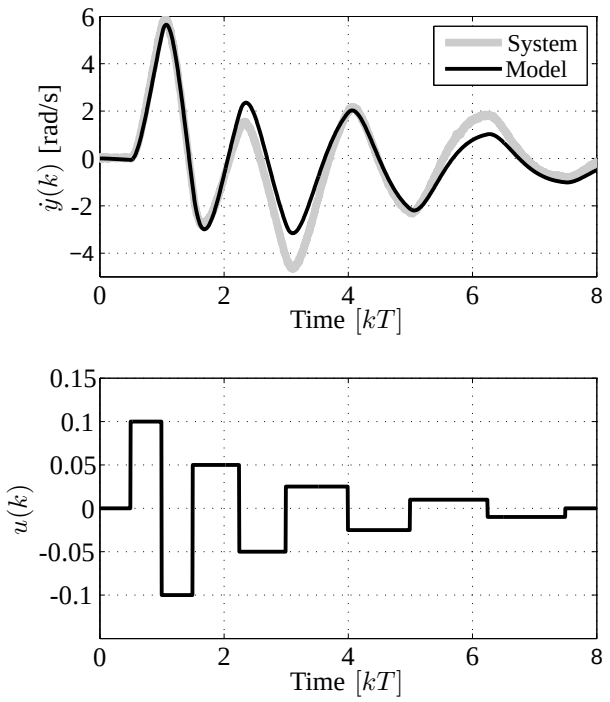

Fig. 1: Experimental data collected for system Identification (ID). Top plot: measured angular velocity $\dot{y}(k)$ and its equivalent $\hat{\dot{y}}(k)$ estimated from the identified model. Bottom plot: input applied during system ID.

where $v_z(t)$ and $v_\psi(t)$ are respectively the altitude and yaw command signals of the vehicle, and v_θ and v_ϕ are the respective roll and pitch commands.

The problem to be considered in this paper is the control of θ and ϕ angles so that a fast tracking performance is achieved while minimizing the disturbance signals $f_{\theta,\phi}$. We assume that the vehicle has a symmetric structure, i.e., $I_\theta = I_\phi = I$ and $b_\theta = b_\phi = b$, so that the same control strategy may be applied to each axis. From (1), it is straightforward to see that both,

$$\begin{aligned} \ddot{\theta} + b\dot{\theta} &= I(v_1 - v_3) + f_\theta \\ \ddot{\phi} + b\dot{\phi} &= I(v_4 - v_2) + f_\phi \end{aligned} \tag{3}$$

may be described by the equivalent transfer function,

$$\frac{Y(s)}{V(s)} = \frac{I}{s(s+b)} \tag{4}$$

where $Y(s)$ is the angle being controlled (either θ of ϕ) and $V(s)$ is the torque applied to the vehicle (respectively, either $v_1 - v_3$ or $v_4 - v_2$). Furthermore, a first order system is used to describe the dynamics between the control signal $U(s)$ sent to the drivers, to the actual torque $V(s)$ generated by the rotor blades, giving rise to the following dynamics,

$$\frac{V(s)}{U(s)} = \frac{k_v}{(s+b_v)}, \tag{5}$$

where k_v and b_v must be identified. Thus, the input-output relation is given by (4) and (5), resulting in the third order transfer function:

$$G(s) = \frac{Y(s)}{U(s)} = \frac{I \cdot k_v}{s(s+b)(s+b_v)}, \tag{6}$$

which relates the input signal $U(s)$ to the angle $Y(s)$.

B. Experimental Setup

The vehicle comprises a 450mm aluminum structure with 10×4.5in blades. A 2200 A/h 3S lypo battery feeds the 30 A ESCs and the 935 rpm/V motors. The control system runs in a 32 bit ARM Cortex M0 from STmicro running at 48 MHz with 128 KByte flash memory. The system is instrumented with an LSM303DLHC three axis accelerometer and an L3GD20 three axis gyroscope that communicate with the Cortex M0 via I^2C protocol.

Since the scope of this paper is limited to the control of the the roll (or pitch) angle of the vehicle, a one degree of freedom experimental setup was developed, i.e., two ends of the quadrotor were fixed so that it could only rotate around the θ (or ϕ) axis. All the plots shown in this paper were experimentally obtained unless explicitly stated otherwise.

C. System Identification

The integrator included in model (6) describes the relation between the angular velocity $\dot{y}$, directly measured by a gyroscope, and the angular position y, estimated from a three-axis accelerometer. Since commercially available gyroscopic sensors usually possess a considerable better signal-to-noise ratio when compared to accelerometers, the former were the sensors of choice while performing system identification experiments on the system. Therefore, the model to be identified is a second order transfer function relating the input signal to the gyroscope sensor, whose discrete-time transfer function may be readily computed by a discretization method, e.g., Euler Forward,

$$\hat{G}_{\dot{y}}(z) = \frac{b_0}{z^2 + za_1 + a_0} \ ,$$

where $b_0 = Ik_vT^2$, $a_1 = T(b + b_v)$ and $a_2 = 1 - T(b + b_v) + bb_vT^2$.

With a sample time of $T = 5$ ms, the data in Fig. 1 was collected and used for system identification. In that figure, the top plot shows the angular velocity $\dot{y}(k)$ and its equivalent $\hat{\dot{y}}(k)$ estimated from the identified model. The bottom plot shows the input sequence – largely based on the work in [18] – applied during identification. A zero phase Butterworth filter with a cut-off frequency of 10 Hz (one tenth of the Nyquist frequency) was used to pre-process the output data[1]. The resulting model is given by,

$$\hat{G}_{\dot{y}}(z) = \frac{0.0231}{z^2 - 1.9776z + 0.9778} \ . \tag{7}$$

It is possible to infer from the figure that the general dynamics of the system was captured by the model. This

[1]This filter was only used in the post-processing of the batch data collected for system identification, and not during the control implementation.

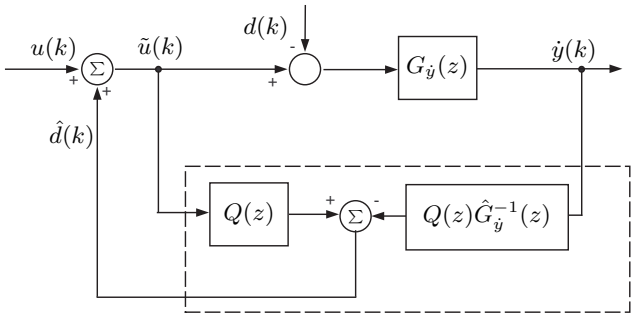

Fig. 2: Discrete time disturbance compensator.

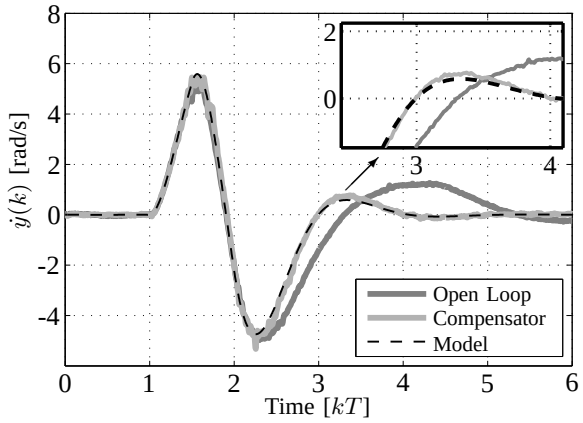

Fig. 3: Validating the system identification and the disturbance observer. Dashed line: model based simulated output; light gray line: experimental data with the disturbance observer; dark gray line: experimental data without the disturbance observer.

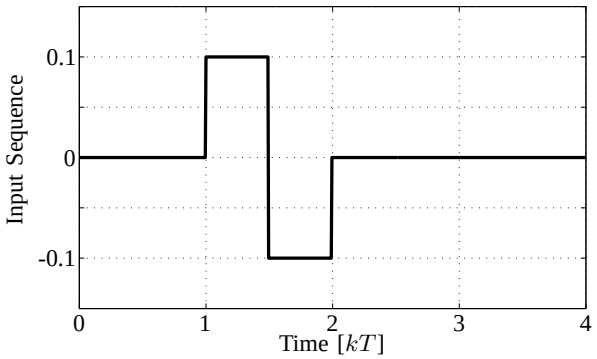

Fig. 4: Sequence of a "Doublet" input [18] generating the outputs in Fig. 3.

model will be used in the implementation of the disturbance observer, described in the next section. Naturally, by integrating equation (7) one finds the relation between the input signal and the angle of the vehicle.

III. Disturbance observer

Multirotor vehicles such as the one studied in this work are subject to several perturbations ranging from wind gusts to actuators interaction with nearby obstacles, as well as unmodeled actuator cross coupling and parametric uncertainties. In order to reduce the uncertainty related to these undesired phenomena, we propose a disturbance observer that allows the separation between the tracking and disturbance rejection tasks. The strategy implemented in this paper is adapted from [19] and depicted in Fig. 2, where $G_{\dot{y}}(z)$ represents the actual system and $\hat{G}_{\dot{y}}(z)$ the approximate model of the system as given in (7). Furthermore, $Q(z)$ is a low pass filter, whose order is greater or equal to that of $\hat{G}_{\dot{y}}(z)$. This filter servers two main purposes: besides making the product $Q(z)\hat{G}_{\dot{y}}^{-1}(z)$ causal, it provides a way of limiting the actuation of the disturbance observer to a desired bandwidth ω_Q, thus avoiding the amplification of noise acting on large frequencies.

It is easy to verify that, in the presence of the disturbance observer and considering that $\hat{G}_{\dot{\theta}}(z) \approx G_{\dot{\theta}}(z)$ in low frequencies (below ω_Q), the following relation holds,

$$\frac{\dot{Y}(z)}{U(z)} = \hat{G}_{\dot{y}}(z)[U_\theta(z) - D(z)(1 - Q(z))] \ ,$$

where $D(z)$ represents the $\mathcal{Z}$-transform of the signal $d(k)$. It is obvious, thus, that by choosing $Q(z)$ as an appropriate low pass filter, the effects of disturbance are eliminated in low frequencies. For this particular application a second order filter was designed such that $\omega_Q = 20$ Hz, that is, 20% of the Nyquist frequency:

$$Q(z) = \frac{b_{q0}}{z^2 + za_{q1} + a_{q0}} = \frac{9.654 \times 10^{-3}}{z^2 - 1.956z + 0.956} \ . \quad (8)$$

Note that the only sensor this compensator uses is the gyroscope because this is a high-gain strategy that requires a good signal-to-noise ratio (SNR) in order to perform well. Once again, the gyroscope possesses a better SNR when compared to the accelerometer, hence this sensor alone is used for the disturbance compensator implementation.

In order to validate the disturbance observer, we have applied the so-called "Doublet" input sequence [18] – depicted in Fig. 4 – both to the open loop system and to the strategy depicted in Fig. 2. The results are seen in Fig. 3 together with the expected output $\hat{\dot{y}}(k)$ given by the model. Disturbances acting on the system, along with unmodeled nonlinear phenomena, are compensated up to a frequency ω_Q chosen according to (8).

In the absence of large model errors, disturbance observers allow independent tuning of disturbance rejection characteristics and reference tracking. Furthermore, they are more flexible than simple integrators and do not remove 90 degrees of phase in the resulting closed loop system. Their tuning is directly based on the bandwidth of the low pass filter and added degrees of flexibility include the Q filter order and relative degree. For this and other reasons, disturbance observers are "particularly helpful in situations where gains need to be tuned on-line" [19].

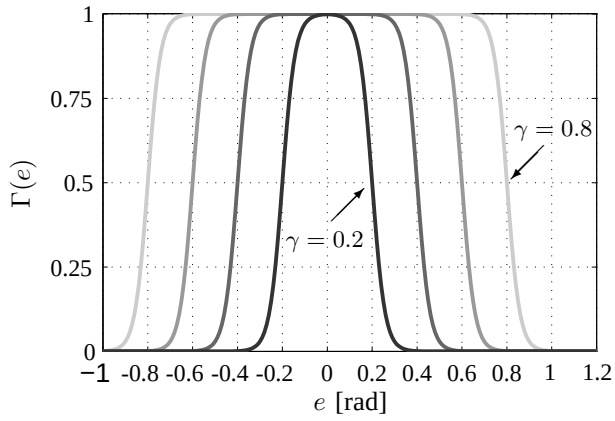

Fig. 5: Function $\Gamma(e)$ in (10) for different values of γ.

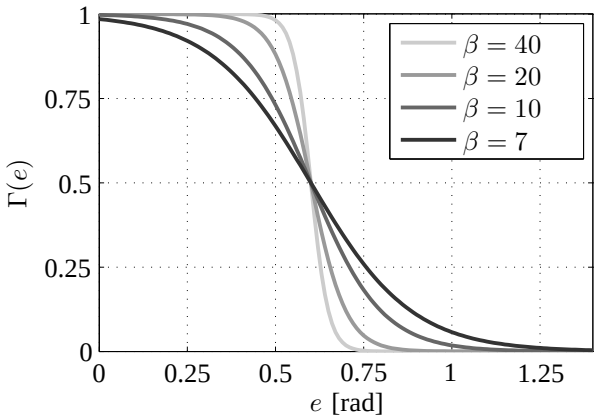

Fig. 6: Function $\Gamma(e)$ in (10) for different values of β.

IV. Nonlinear Control

Every control law designed for rapid reference tracking will face the fundamental limitations given by the system being controlled. The most common of such limitations are related to actuator saturation and to a limited bandwidth available for the system [20]. The latter is due to a series of factors related to the sampling rate, the dynamic limits of the actuators, the so called *water bed effect* [21], among others. While some of these limits impose hard constraints on the system performance, others may be "stretched" through techniques of nonlinear control. Since the system considered in this paper is primarily limited by bandwidth limitations imposed by the sensors, this is the problem dealt with by the nonlinear control to be applied.

In order to reduce the tracking time of the system without requiring a larger bandwidth, we propose the implementation of a nonlinear gain-scheduled PD controller. Its objective is the dynamic allocation of the closed-loop poles as a function of the tracking error. For large values of the tracking error, it is desirable that an undamped behavior is given to the system, so that it possesses a fast rise time. As the system reaches the reference level, however, a damped behavior is necessary so that excessive levels of overshoot are avoided. Controllers that dynamically add damping to the system are referred to as *nonlinear damping* [17], or Composite Nonlinear Feedback [22], and may be implemented in the following form:

$$u(k) = e(k) \cdot k_p - \dot{y}(k)(k_{du} + k_{dd} \cdot \Gamma(e(k))) \qquad (9)$$

where $e := y - r$ is the tracking error and k_{du} and k_{dd} are such that $k_{dd} > k_{du} > 0$.

This controller is tunned by choosing a proportional gain $k_p > 0$ such that the system achieves the desired bandwidth. This gain may be computed using the root-locus method such that the system becomes marginally stable, for instance. Afterwards, derivative gains k_{dd} and k_{du} are sought such the system becomes significantly damped, respectively undamped, in a PD type closed loop. With these gains in hand a smooth function $\Gamma(e)$ is used in order to switch the system behavior – from undamped to damped – as the error approaches zero. In other words, the switching function is designed such that: (i) the system presents an undamped behavior given by k_{du} when far from the reference; (ii) the systems presents a damped behavior given by k_{dd} as it approaches the reference. The nonlinear function $\Gamma(e)$ is responsible for the dynamic pole placement, since this function must be close to zero for large values of e, and close to one for $|e| \approx 0$, a possible choice is given by,

$$\Gamma(e) = \left(1 - \frac{1}{1 + \mathrm{e}^{\beta(\gamma - |e|)}}\right). \qquad (10)$$

This function is plotted in Fig. 5 where it is clear that $|e| >> 0$ implies $\Gamma(e) = 0$, and $|e| \approx 0$ implies $\Gamma(e) = 1$. Parameters γ and β respectively determine the point where the transition from zero to one happens (Fig. 5), and the inclination of such transition (Fig. 6). As a result, the closed loop system will present a fast rise time without overshoot, improving its dynamic response without increasing the overall bandwidth.

The control gains were chosen according to the root locus method and are given by, $k_p = 0.1$, $k_{dd} = 0.1$ and $k_{du} = 0.01$. The nonlinear function parameters were determined empirically, and fixed at $\beta = 35$ and $\gamma = \pi/4$.

V. Implementation

In order to implement the control strategy in (9), it is necessary to use measurements from the output angle $y = \theta$ (or $y = \phi$) and its time derivative $y = \dot{\theta}$ (or $y = \dot{\phi}$). Since the gyroscope directly measures angular velocity, it is ready to be used in the control law. The accelerometer, on the other hand, measures linear acceleration and its signal must be processed in order to provide the output angle y. A simple sensor fusion technique will be described next section in order to estimate the correct inclination of the vehicle.

A. Complementary Filters

By measuring the linear accelerations of the vehicle it is possible to infer the forces acting on it. In particular, when the vehicle is at constant linear speed, the only external force acting on it is the gravitational one. It is, then, possible to estimate the vehicle inclination with respect to an earth fixed

frame, according to,

$$\hat{y}_a = \begin{cases} \arctan\left(\frac{a_y}{\sqrt{a_x^2+a_z^2}}\right), & \text{for } y=\theta, \\ \arctan\left(\frac{a_x}{\sqrt{a_y^2+a_z^2}}\right), & \text{for } y=\phi, \end{cases} \quad (11)$$

where a_x, a_y e a_z are the linear accelerations at axis x, y and z as given by the accelerometer. However, when the vehicle is accelerating in any given direction or when noise is present in the measurements, these estimates will present significant errors.

A second approach to estimate y consists in the direct integration of the gyroscope. Numerically this is performed in the simple form,

$$\hat{y}_g = \frac{Tz}{z-1}\dot{y} \quad (12)$$

where $\hat{y}_g$ is the estimate of y (either θ or ϕ) obtained from the gyroscope (respectively either $\dot{\theta}$ or $\dot{\phi}$). However, as usual with any process of numerical integration, any biased noise will cause this estimate to drift.

It is, therefore, clear that the estimate of the output angles from any of these sensors acting alone will cause problems: while high frequency noise, along with measurements caused by any acceleration other than gravity, affects the estimate of $\hat{y}_a$ given by the accelerometer alone; low frequency bias will cause the gyroscope estimate $\hat{y}_g$ to drift. Ideally, one would like to use the gyroscope only in high frequencies, and the accelerometer only in low frequencies. Hence the idea behind complementary filters, which are defined as any pair of filters such that $A(z) + B(z) = 1$. In this particular case,

$$A(z) = \frac{z(1-p)}{z-p}, \quad B(z) = \frac{p(z-1)}{z-p}.$$

That is, filter $A(z)$ is a low pass filter which will be used in the estimate of $\hat{y}_a$, and $B(z)$ is a high pass filter applied to $\hat{y}_g$. The filter equation becomes,

$$\hat{Y}(z) = A(z)\hat{Y}_a(z) + B(z)\hat{Y}_g(z), \quad (13)$$

which, by making use of (12), may be implemented by the simple equation:

$$\hat{y}(k) = p \cdot \hat{y}(k-1) + (1-p) \cdot \hat{y}_a(k) + pT \cdot \dot{y}(k), \quad (14)$$

where p is a tuning parameter.

B. Experimental Results

In order to validate the proposed approach, the system was subject to a step-like reference taking it from the origin $\dot{y}(0) = y(0) = 0$ to the $y = 1$ rad and $\dot{y} = 0$. In order to illustrate the benefits of the proposed approach, four experiments were performed, as exposed in Figures 7 and 8:

1) the closed loop system using the nonlinear control law as given in (9) (black line) is presented in both figures;
2) Fig. 7 also shows two linear PD controllers – with $u(k) = k_p \cdot e - k_d \cdot \dot{y}(k)$ as opposed to (9) – for the undamped case with $k_d = 0.02$, and for the damped case with $k_d = 0.09$;

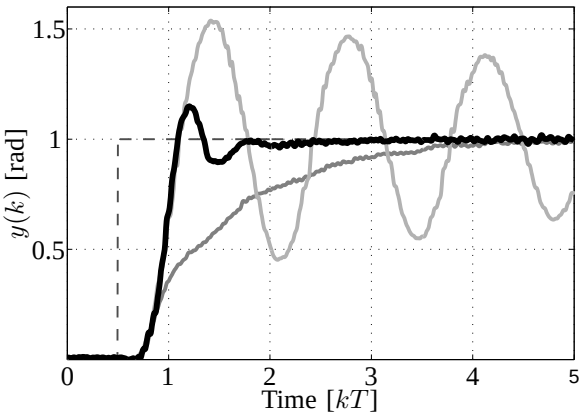

Fig. 7: System response to the different control laws from the origin to $r = 1$ rad. Legend: black line - proposed controller; light grey line - undamped controller; dark grey line - damped controller.

3) Fig. 8 shows the behavior of a linear PD controller achieving the same level of overshoot as the nonlinear controller due to the meticulous choice of $k_d = 0.033$;

From Fig. 7 it is possible to verify the benefits of the proposed approach. Note that, as expected, the undamped closed loop system generates a fast rise time but unacceptable oscillatory behavior around the reference, resulting in a system with poor performance. On the other hand, the damped closed loop system presents no overshoot at all, but its dynamic response is too slow. By selecting the best traits of these linear controllers, the proposed control law is able to achieve a fast rise time with small levels of overshoot and oscillation, significantly improving the system performance when compared to the linear controllers.

In order to explicit the fact that no PD gain combination is able to achieve a better response, Fig. 8 shows a comparison between the proposed controller and a linear PD that was specifically tuned to achieve the same overshoot as the proposed one. It is clear that a linear controller tuned for the same overshoot takes over twice as much time to accommodate as its nonlinear counterpart. This is about the same time required by the damped PD controller, and the best performance we were able to achieve with the PD topology.

VI. Conclusion

This paper has developed a nonlinear discrete time control strategy for the fast tracking of quadrotor-like vehicles. In order to aid the system with respect to disturbance rejection and to reduce the effects of unmodeled dynamics, a disturbance observer was implemented. Experimental results have shown that the disturbance observer improves the system behavior by also eliminating the effects of unmodeled dynamics, thus generating a better fit between the system and the model. The proposed nonlinear controller introduced a dynamic damping term to the closed loop system so that the a fast rise time response is achieved with limited levels of overshoot. Experimental results have been presented showing

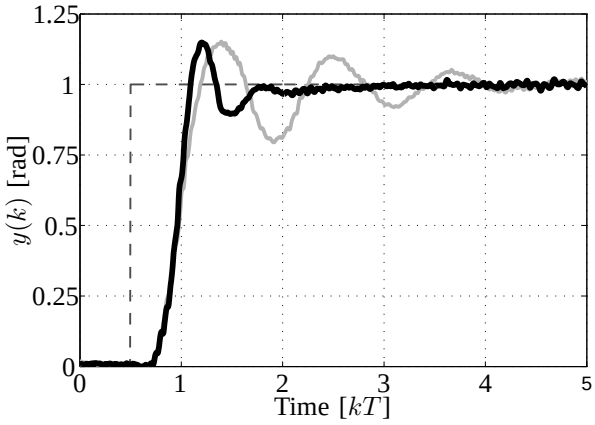

Fig. 8: A linear controller with $k_d = 0.03$ achieves the same overshoot as the nonlinear control law, but takes a considerably longer time to accommodate.

that the superiority of the proposed method when compared to traditional linear methods. A significantly faster tracking time was achieved.

Our future work will focus on the improvement of the remaining degrees of freedom of the system. When all control loops are working simultaneously, it may be important to consider saturation in the actuators. Different methods may be investigated, such as the Proximate Time Optimal Servomechanism [23] and its dynamically damped version [24].

ACKNOWLEDGMENT

This work was partially supported by FAPERGS and CNPq, Brazil, under grants 13/1896-1 and 443979/2014-6 respectively.

REFERENCES

[1] M. Funaki, S.-I. Higashino, S. Sakanaka, N. Iwata, N. Nakamura, N. Hirasawa, N. Obara, and M. Kuwabara, "Small unmanned aerial vehicles for aeromagnetic surveys and their flights in the south shetland islands, antarctica," *Polar Science*, vol. 8, no. 4, pp. 342–356, 2014.

[2] M. Dunbabin and L. Marques, "Robots for environmental monitoring: Significant advancements and applications," *Robotics & Automation Magazine, IEEE*, vol. 19, no. 1, pp. 24–39, 2012.

[3] V. V. Klemas, "Coastal and environmental remote sensing from unmanned aerial vehicles: An overview," *Journal of Coastal Research*, 2015.

[4] J. Bellvert, P. Zarco-Tejada, J. Girona, and E. Fereres, "Mapping crop water stress index in a ?pinot-noir?vineyard: comparing ground measurements with thermal remote sensing imagery from an unmanned aerial vehicle," *Precision agriculture*, vol. 15, no. 4, pp. 361–376, 2014.

[5] S. Martin, F. Beyrich, and J. Bange, "Observing entrainment processes using a small unmanned aerial vehicle: A feasibility study," *Boundary-layer meteorology*, vol. 150, no. 3, pp. 449–467, 2014.

[6] C. Deng, S. Wang, Z. Huang, Z. Tan, and J. Liu, "Unmanned aerial vehicles for power line inspection: A cooperative way in platforms and communications," *Journal of Communications*, vol. 9, no. 9, 2014.

[7] J. Martinez-de Dios, K. Lferd, A. de San Bernabé, G. Núñez, A. Torres-González, and A. Ollero, "Cooperation between uas and wireless sensor networks for efficient data collection in large environments," *Journal of Intelligent & Robotic Systems*, vol. 70, no. 1-4, pp. 491–508, 2013.

[8] S. Siebert and J. Teizer, "Mobile 3d mapping for surveying earthwork projects using an unmanned aerial vehicle (uav) system," *Automation in Construction*, vol. 41, pp. 1–14, 2014.

[9] A. Wada, T. Yamashita, M. Maruyama, T. Arai, H. Adachi, and H. Tsuji, "A surveillance system using small unmanned aerial vehicle (uav) related technologies," *NEC Technical Journal*, vol. 8, no. 1, pp. 68–72, 2015.

[10] F. Kendoul, "Survey of advances in guidance, navigation, and control of unmanned rotorcraft systems," *Journal of Field Robotics*, vol. 29, no. 2, pp. 315–378, 2012.

[11] G. Hoffmann, D. G. Rajnarayan, S. L. Waslander, D. Dostal, J. S. Jang, and C. J. Tomlin, "The stanford testbed of autonomous rotorcraft for multi agent control (starmac)," in *Digital Avionics Systems Conference, 2004. DASC 04. The 23rd*, vol. 2. IEEE, 2004, pp. 12–E.

[12] J. P. How, B. Bethke, A. Frank, D. Dale, and J. Vian, "Real-time indoor autonomous vehicle test environment," *Control Systems, IEEE*, vol. 28, no. 2, pp. 51–64, 2008.

[13] S. Lupashin, A. Schollig, M. Hehn, and R. D'Andrea, "The flying machine arena as of 2010," in *Robotics and Automation (ICRA), 2011 IEEE International Conference on*. IEEE, 2011, pp. 2970–2971.

[14] A. Bemporad, C. A. Pascucci, and C. Rocchi, "Hierarchical and hybrid model predictive control of quadcopter air vehicles," in *Analysis and Design of Hybrid Systems*, vol. 3, no. 1, 2009, pp. 14–19.

[15] B. M. Chen, T. H. Lee, K. Peng, and V. Venkataramanan, "Composite nonlinear feedback control for linear systems with input saturation: theory and an application," *Automatic Control, IEEE Transactions on*, vol. 48, no. 3, pp. 427–439, 2003.

[16] Z. Lin, M. Pachter, and S. Banda, "Toward improvement of tracking performance nonlinear feedback for linear systems," *International Journal of Control*, vol. 70, no. 1, pp. 1–11, 1998.

[17] J. B. Lewis, "The use of nonlinear feedback to improve the transient response of a servomechanism," *Transactions of the American Institute of Electrical Engineers, Part II: Applications and Industry*, vol. 71, no. 6, pp. 449–453, 1953.

[18] M. F. Shafer, *Flight investigation of various control inputs intended for parameter estimation*. National Aeronautics and Space Administration, Ames Research Center, Dryden Flight Research Facility, 1984, vol. 85901.

[19] C. J. Kempf and S. Kobayashi, "Disturbance observer and feedforward design for a high-speed direct-drive positioning table," *Control Systems Technology, IEEE Transactions on*, vol. 7, no. 5, pp. 513–526, 1999.

[20] G. Stein, "The practical, physical (and sometimes dangerous) consequences of control must be respected, and the underlying principles must be clearly and well taught." *IEEE Control Systems Magazine*, vol. 272, no. 1708/03, 2003.

[21] M. M. Seron, J. H. Braslavsky, and G. C. Goodwin, *Fundamental Limitations in Filtering and Control*. London: Springer-Verlag, 1997.

[22] Z. Lin, M. Pachter, and B. S., "Toward improvement of tracking performance-nonlinear feedback for linear systems," *Int. Journal of Control*, vol. 70, pp. 1–11, 1998.

[23] L. Y. Pao and G. F. Franklin, "Proximate time-optimal control of third-order servomechanisms," *Automatic Control, IEEE Transactions on*, vol. 38, no. 4, pp. 560–580, 1993.

[24] A. T. Salton, Z. Chen, and M. Fu, "Improved control design methods for proximate time-optimal servomechanisms," *Mechatronics, IEEE/ASME Transactions on*, vol. 17, no. 6, pp. 1049–1058, 2012.